A Rheological Method to Describe Metastable Hydrate-in-Oil Slurries

*Yahua Qin, Paul F. Pickering, Michael L. Johns, Eric F. May, Zachary M. Aman**

Fluid Science & Resources, Department of Chemical Engineering, The University of Western Australia, Crawley, Western Australia 6009, Australia

Abstract

Gas hydrates are ice-like solids, which may form and aggregate in crude oil pipelines; in severe cases, the increase in frictional pressure drop may exceed the available driving force, resulting in a non-flowing (blockage) condition. In order to assess the severity of hydrate formation in oil- or condensate-dominant lines, a slurry viscosity model must be applied to, and validated for, hydrate-laden suspension. A well-known model, applied in industrial situations for hydrate slurry rheology has been suggested to significantly under-predict apparent viscosity during the early and intermediate stages of hydrate blockage formation. As hydrate particles suspended in the slurry may aggregate, this study interrogates their suspension rheology in two parts: the underlying suspension behavior was tested by injecting industrial anti-agglomerant (AA) chemicals, thereby identifying the contribution of particle aggregation for identical systems without AAs. A temperature-controlled high-pressure rheometer with a vane blade rotor was deployed, where hydrate-in-oil suspensions were formed from a metastable water-in-oil emulsion pressurized with methane. The results first illustrate that, at similar operating conditions, the addition of AAs reduced the hydrate growth rate by an order of magnitude and decreased the steady-state relative viscosity order of magnitude. After the hydrate volume fraction achieved a steady-state condition, the addition of AA suppressed the magnitude of the hydrate-in-oil slurry viscosity flow curve by an order of magnitude. Extrapolated to infinite shear rate, the apparent viscosity behavior of hydrate-in-oil suspensions was compared with a range of rheological suspension models. The current industry model was indeed found to perform poorly, which may be due to assumptions of rigid and spherical particles; a revised suspension model considering arbitrarily-shaped particles improved experimental predictions by between 50 and 60% for two crude oil systems.

Keywords: *hydrate anti-agglomerants, slurry viscosity, particle aggregation, flow assurance*

1 INTRODUCTION

In subsea oil and gas pipelines, the rapid cooling of gas and liquid water under high pressure enables the formation of solid inclusion compounds known as clathrate hydrates,[1] which may suspend in the oil phase and, under limited operating conditions, form hydrate-in-oil suspensions. Hydrate formation has a deleterious impact on the safety and effectiveness of hydrocarbon transportation in pipelines[2] and can result in increases to suspension viscosity[3] that, as can be derived form a simple momentum balance, increase frictional pressure loss during flow.[4-5] In the limit that this pressure loss approaches or exceeds the available differential pressure in the pipeline, a reduction in flow velocity toward a non-flowing ("plugged") condition is expected.

To assess the hydrate blockage formation risk, slurry viscosity has been identified as a critical parameter[6-7] alongside multiphase flow contributions to the momentum balance, including heterogeneous particle distributions, moving or stationary bed formation, or film growth at the wall; the development of a universal model that can predict the hydrate-in-oil viscosity accurately is thus of great significance. Some efforts have been made in this regard, with approaches generally focusing on two areas: (i) direct application of the conventional rheological models for fluids with data fitting, or other empirical approaches based on these rheological models; and (ii) model establishment based on fundamental principles of suspensions. The former has been widely applied over a range of experimental systems and conditions. For example, the power law model was used to describe the rheological properties of ambient pressure cyclopentane hydrate slurries in a rheometer[8-9] and a flowloop,[10] as well as high pressure methane hydrate slurries in crude oil[11] and mineral oil.[12] The Cross model[13] was applied to quantify the rheology of methane hydrate slurries formed from AOT/water/oil emulsions,[14] while the Herschel-Bulkley model was adopted[15] for the description of CO_2 hydrate slurry flow[16] including with the presence of additives[17] in a dynamic loop. The Bingham [18] model was employed for the description of TBAB hydrate slurries[19] and methane hydrate in a flowloop.[20] A semi-empirical approach based on the Herschel-Bulkley model was also established to describe the rheology of TBAB hydrate slurries[21] and a natural gas hydrate slurry containing anti-agglomerant in a flowloop.[22]

Although these empirical and semi-empirical approaches enable estimates of hydrate slurry viscosity, the limitation exists that any conclusions drawn are applicable only to the specific experimental conditions under which the data were derived. This lacks universality and prevents the models from being employed within the multiphase flow simulators used by industry. To overcome this limitation, a model based on the physical analysis of slurry formation and flow is necessary. Camargo and Palermo[23] first addressed this in 2002 by analyzing the rheological properties of hydrate suspensions in an asphaltenic crude oil with both a flow loop and a rheometer and proposing a predictive model. This was extended by Sinquin et al. [24] and improved by Palermo et al.,[25] Fidel-Dufour et al.[26] and Colombel et al.[27] through the incorporation of population balance; although the improved model is used commonly in the industry, limited research has been published to inform its accuracy.[23-24]

Boxall et al.[28,29] presented an example of how a suspension rheology model, informed by multiphase surface area and hydrate kinetic predictions, may be used to assess the severity of hydrate blockage formation in oil-continuous flowlines.

The original model is comprised of three main parts: (i) a basic rheological model for concentrated suspensions of equally sized hard spheres, accounting only for hydrodynamic interactions;[30] (ii) adaptation of the rheological model for aggregated concentrated suspensions, with the assumption that the hydrate aggregates are fractal;[31-32] and (iii) the maximum aggregate size determination, which depends on the balance between shear stress and force of adhesion between particles.[33-34] In order to improve the model, these three parts should be individually assessed. It is obvious that the aggregation of hydrate particles is considered only in the latter two parts of the model; the basic rheological model that serves as the first component only considers suspensions in which hydrate particles are separated and not aggregated. Thus, the accuracy of this underlying model can be tested if aggregation is prevented. This can be achieved through the use of anti-agglomerants (AAs), which inhibit aggregation between hydrate particles due to the presence of amphiphilic molecules, where the hydrophilic head of the AA adsorbs to the hydrate-oil interface, and the lipophilic tail causes the crystals to become oil-wet and therefore easily dispersible in the liquid oil phase.[1, 35] Hence, the systematic addition of AA enables assessment of the rheological properties of discrete hydrate-in-oil suspensions; these data can then be used to verify the accuracy of the underlying model.

In this work, rheological measurements of methane hydrate slurries formed from water-in-oil emulsions containing AAs were conducted using a controlled-stress, high-pressure rheometer. Emulsions of varying water cuts ranging from 5% to 30% were formed with two crude oils of different viscosities. Infinite shear viscosity data were extrapolated from flow curves, and were compared with basic suspension rheology models[30] to assess industrial applicability.

2 METHODS

2.1 Emulsion Preparation and Characterization

Water-in-oil emulsions were prepared from deionized water, industrial AA and crude oil. Before making the emulsions, the mass and density of the crude oil were measured and the desired amount of deionized water was determined to achieve target volume fractions ranging from 0.05 to 0.30 for each test. The amount of AA added to the crude oil phase was set to be 2 wt% of the amount of water to be used when forming the emulsion. The AA was combined with the crude oil and the resulting mixture was shaken by hand. Finally, the water was added dropwise into the crude oil and AA mixture while vigorously stirring with a homogenizer, similar to procedures described previously.[36] Density and viscosity data for both dead crude oils and live oils (dead crude oils saturated with methane under pressure) are given in Table 1.

Table 1. Properties of the Australian crude oils used for this investigation.

	Dead oil			Live oil (7.5 MPa)	
	Density (kg/m^3) at 20°C	Viscosity (mPa.s) at 20°C	Viscosity (mPa.s) at 1°C	Viscosity (mPa.s) at 1°C	Viscosity (mPa.s) at 5°C
Oil A	812	6.8	60	18.5	11.5
Oil B	900	128	598	108	92.8

The size distribution of water droplets was determined with a Magritek 1 T Halbach Array permanent magnet and spectrometer, with a 1 T/m magnetic field gradient. The specific measurement principles and procedures were described in detail previously by Johns and co-workers.[37-39] By way of example, Figure 1 shows the evolution in measured droplet size distribution with water cuts from 0.05 to 0.30 for crude oil B in the absence of AAs.

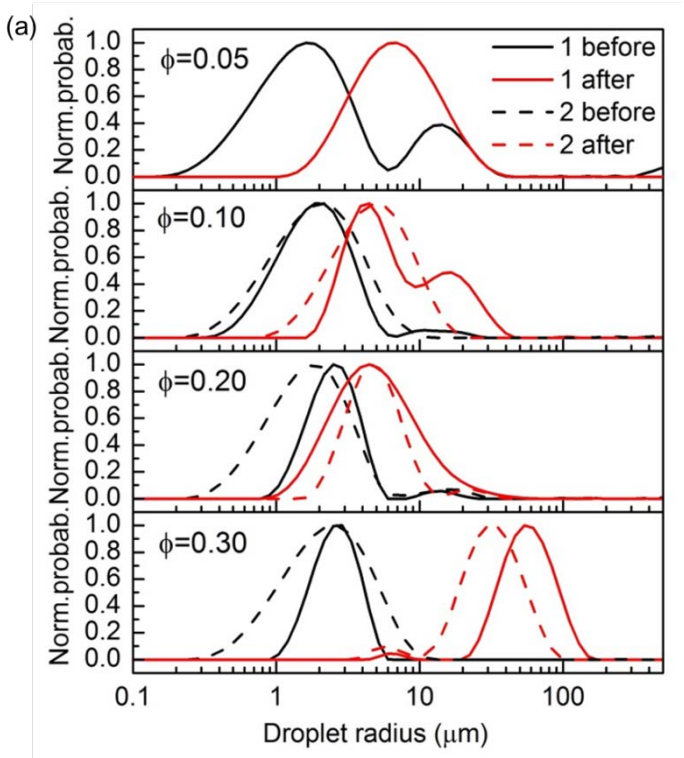

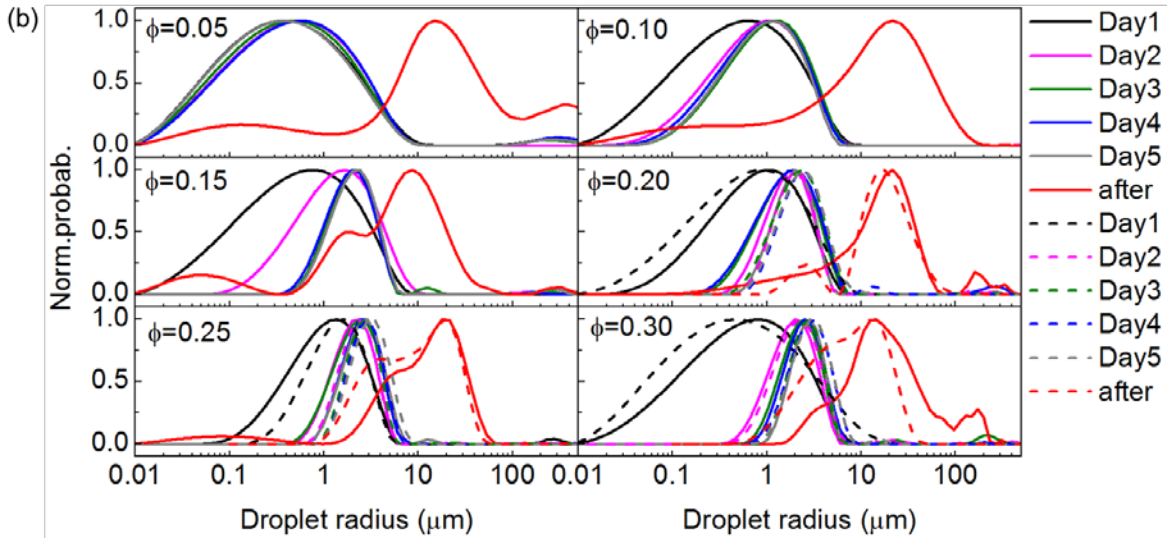

Figure 1. (Panel A) NMR emulsified droplet size distributions for two trials (1 and 2) before hydrate formation (solid black and dashed black curves) and after hydrate dissociation (solid red and dashed red curves) for 0.05, 0.10, 0.20, and 0.30 watercut emulsions generated with Oil A. (Panel B) NMR emulsified droplet size distributions as a function of time after generation, in the absence of hydrate formation (black, pink, green, blue and grey curves), compared with systems after hydrate dissociation (red curves) for 0.05, 0.10, 0.15, 0.20, 0.25 and 0.30 watercut, respectively, generated with oil B; dashed lines represent repeat trials of 0.20, 0.25, 0.30 watercut emulsions.

2.2 High Pressure Hydrate Rheometer System

Controlled stress rheometers have the advantage of providing direct measurement of the shear stress of fluids under a controlled shear rate, but have conventionally been limited to mixing systems (i.e. concentric cylinders) that are unable to maintain solution gas during hydrate growth. The vane blade mixing system in this rheometer readily maintains solution gas, replicating the conditions encountered in subsea oil pipelines, enabling the assessment of apparent slurry viscosity as a function of hydrate volume fraction. Data interpretation and the assumptions associated therewith are described by Qin et al.[40] (**Figure 2**), wherein the measurement system was comprised of a chiller, a syringe pump, a gas manifold and a controlled-stress rheometer with a high-pressure cell, was also used for this research. The high-pressure cell included a Peltier jacket, a stainless-steel cell, a rotor and magnetic coupling system, with maximum pressure rated to 13.8 MPa and a temperature range of −10 to 150 °C when connected to the chiller for heat removal. A vane-type rotor was used as this was able to maintain saturation of the crude oil phase and deliver excellent repeatability between independent trials in previous tests. The rheometer was connected to an Isco syringe pump, the maximum volume of which was 260 mL, to ensure constant pressure during methane saturation of the emulsion. In this work, gas hydrates were formed inside the stainless-steel cell after which isochoric, high-pressure, in-situ rheological measurements of the resulting slurries were conducted.

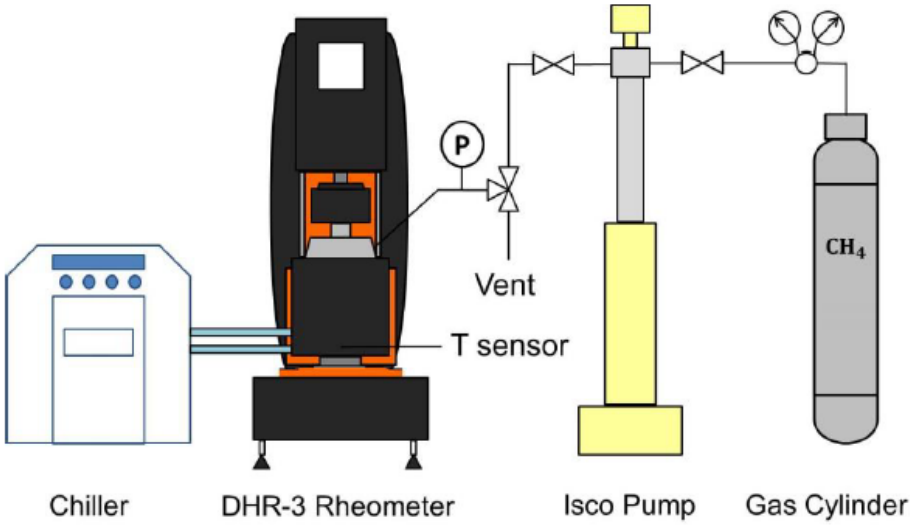

Figure 2. Schematic of the high-pressure rheometer assembly.

For each test, the emulsion prepared at atmosphere pressure was transferred into the high-pressure cell and stirred at a shear rate of 217 s^{-1} whilst the cell was charged with 10 MPa methane. This occurred until the oil was fully saturated with methane as indicated by no further change in the volume of the syringe pump. The rheometer was subsequently isolated from the Isco syringe pump by closing the connecting valve. Thereafter, the rheological properties of the suspensions were recorded throughout three stages: (i) transient hydrate formation; (ii) steady-state hydrate slurry with full water conversion; and (iii) system restart after an eight-hour simulated shut-in process. The specific procedures were as follows:

1. The methane-saturated emulsion was cooled isochorically from 20 °C and 10 MPa to 1 °C at 0.5 °C/min to generate a driving force for hydrate formation. The shear rate during this process was 43.5 s^{-1}.
2. The apparent suspension viscosity was measured during the hydrate growth period under a constant shear rate (43.5 s^{-1}); the measurement continued for 12 hours after the pressure signal reached steady-state, to ensure the primary hydrate growth period had reached completion.
3. A flow curve was measured at 1 °C for the steady-state hydrate-in-oil suspension, where the shear rate was reduced stepwise from 43.5 s^{-1} to 4 s^{-1}, taking 50 shear rate points per decade. The shear rate was then increased to 220 s^{-1} over 50 points, and then decreased again to 4 s^{-1} over 50 points. As the suspensions displayed varying degrees of thixotropy, the apparent suspension viscosity was monitored at each shear rate, and the steady-state value was used in the flow curve; steady-state was defined when the deviation between three sequential measurements was less than 5 %.
4. The temperature was increased to 5 °C while the system was subject to a constant shear rate (43.5 s^{-1}), and was then held at this condition for 30 minutes. After this period, the flow curve measurements described in step 3 were performed again.
5. To simulate the effect of subsea shut-in, the hydrate slurry was permitted to anneal at 5 °C for eight hours under 1 Hz frequency oscillations at 2% strain, according to the procedure described by Webb et al.[11]

6. After annealing, the yield stress of the hydrate-in-oil suspension was measured by increasing the applied shear stress from 0.1 to 300 Pa over 1080 s at a constant temperature (5 °C); the analysis procedure used for the yield stress measurements is discussed below.

3 RESULTS AND DISCUSSION

3.1 Apparent Viscosity during Hydrate Growth

The cell pressure, temperature and apparent viscosity of the suspension were recorded with time during the hydrate formation process for each test. **Figure 3** shows an example of oil A systems of the same water cut, with and without AA. In this work, relative viscosity is defined as the ratio of the apparent viscosity of the suspension to the viscosity of the methane-saturated oil phase (**Table 1**) prior to hydrate formation.

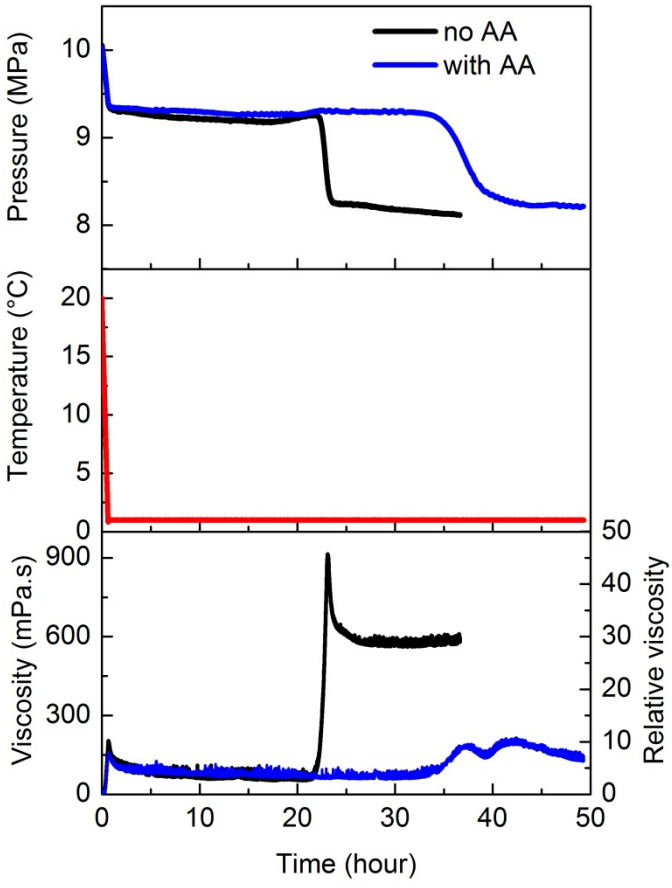

Figure 3. Pressure, temperature and viscosity profiles of a methane-saturated water-in-oil A emulsion (0.20 water cut), with and without AA, at a shear rate of 43.5 s^{-1}, where hydrate formation was detected by a simultaneous decrease in pressure and increase in viscosity (21 hours for system with no AA and 33 hours for system with AA).

For both of these systems, an simultaneous pressure decrease and viscosity increase were observed as the system temperature was reduced from 20 to 1 °C prior to hydrate formation; the subcooling from hydrate equilibrium at 1 °C was 11.5 °C.[41] After reaching 1 °C, hydrate formation was identified by a dramatic pressure decrease and corresponding apparent viscosity increase, with an induction time of 21 hours without AA and 33 hours with AA (**Figure 3**). The pressure decrease corresponded to gas consumption during hydrate growth in the isochoric system, while the apparent viscosity increase was due to the conversion of deformable water droplets to solid hydrate particles. Without AA, the relative viscosity observed during hydrate growth was an order of magnitude higher than when AA was present, highlighting the impact of particle cohesion and aggregation in hydrate systems.[2] Similar to observations in the literature,[11-12, 14] the apparent viscosity of the suspensions decreased with time after reaching a peak value, which may be a result of further structural rearrangement of the hydrate aggregates under mixing.

Compared to the system without AA, the pressure decrease in the AA system occurred at a much slower rate, despite reaching the same steady-state pressure after the cessation of hydrate growth (**Figure 3**). The fractional water conversion to hydrate as a function of time after hydrate nucleation was calculated from the measured pressure decrease and is shown in **Figure 4**. This result suggests that the addition of AA led to a reduction in hydrate growth rate, without affecting the total amount of hydrate formed in the system; as AAs decrease water-oil interfacial tension and tend to increase water-oil interfacial area,[42] the observation of decreased growth rate is likely an energetic penalty arising from surfactant rejection along the growing hydrate interface. Further, the addition of AA decreased the sensitivity of relative viscosity to hydrate volume fraction by an order of magnitude (**Figure 5**).

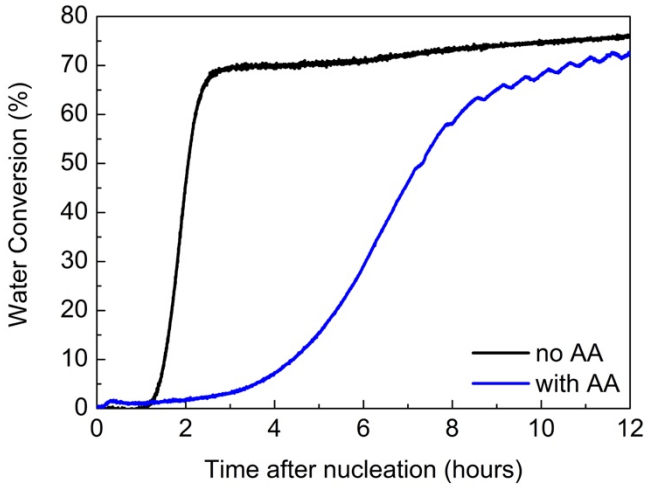

Figure 4. Water conversion percentage as a function of time after hydrate nucleation for water-in-oil A emulsion at 0.20 water cut with and without AA, at a constant temperature (1 °C), shear rate (43.5 s^{-1}) and initial pressure (10 MPa at 20 °C).

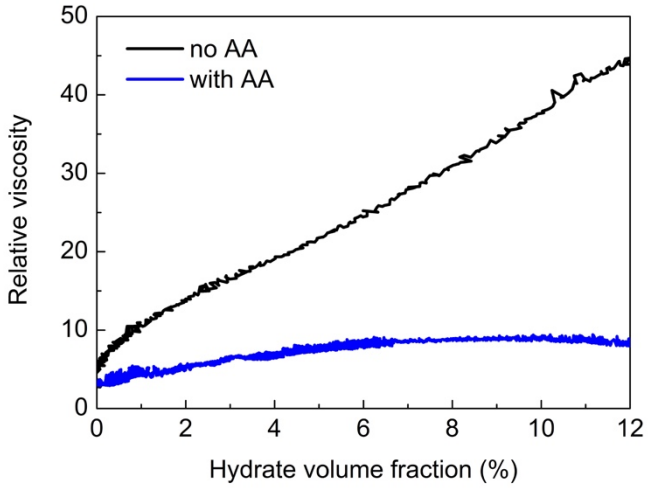

Figure 5. Relative viscosity as a function of hydrate volume fraction for water-in-oil A emulsion at 0.20 water cut with and without AA, at a constant temperature (1 °C), shear rate (43.5 s^{-1}) and initial pressure (10 MPa at 20 °C).

3.2 Apparent Viscosity Dependence on Shear Rate

After hydrate conversion reached a steady-state, apparent viscosities of the hydrate-in-oil slurries formed from emulsions with AA, over a shear rate range from 4 to 220 s^{-1}, with varying water cuts and temperatures of 1 and 5 °C, were recorded, as shown in **Figure 6** for oil A and **Figure 7** for oil B. The suspensions show shear thinning behavior at each water cut tested, where the flow curve shifted to higher viscosity with increasing hydrate volume fraction. The apparent viscosity with decreasing shear rate was fitted as a function of shear rate with the Cross model:[13]

$$\frac{\eta - \eta_\infty}{\eta_0 - \eta_\infty} = \frac{1}{1 + (K\dot{\gamma})^m} \quad (1)$$

where η_∞ is the viscosity at infinite shear, η_0 is the viscosity at zero shear rate, K is a constant parameter with the dimension of time and m is the slope of the shear-thinning regime. The fitting parameters are shown in **Table 2** for oil A and **Table 3** for oil B.

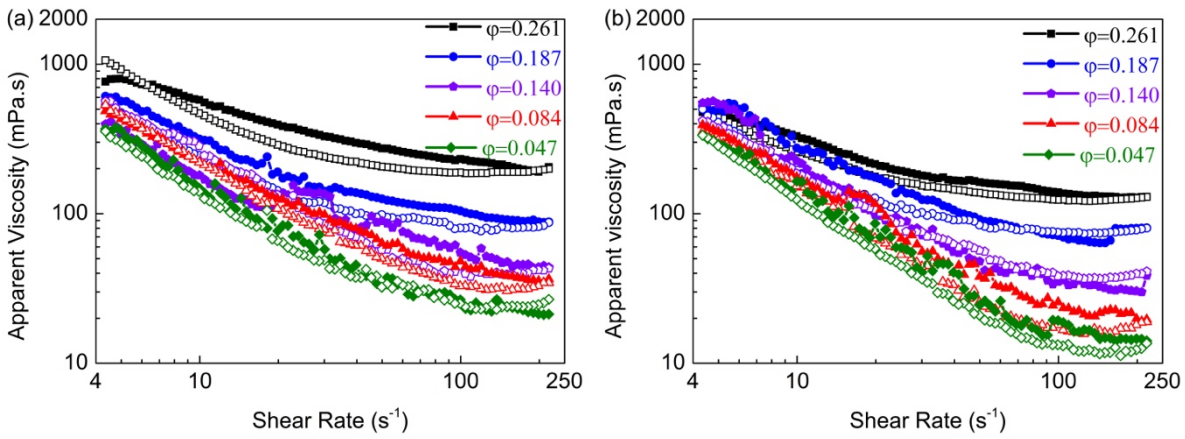

Figure 6. Steady state flow curves of hydrate slurries formed from water-in-oil A emulsions with AA and various water cuts at 1 °C (Panel a) and 5 °C (Panel b). The initial methane pressure prior to hydrate formation and cooling was 10 MPa. Filled data points indicate increasing shear rate, while open data points correspond to decreasing shear rate.

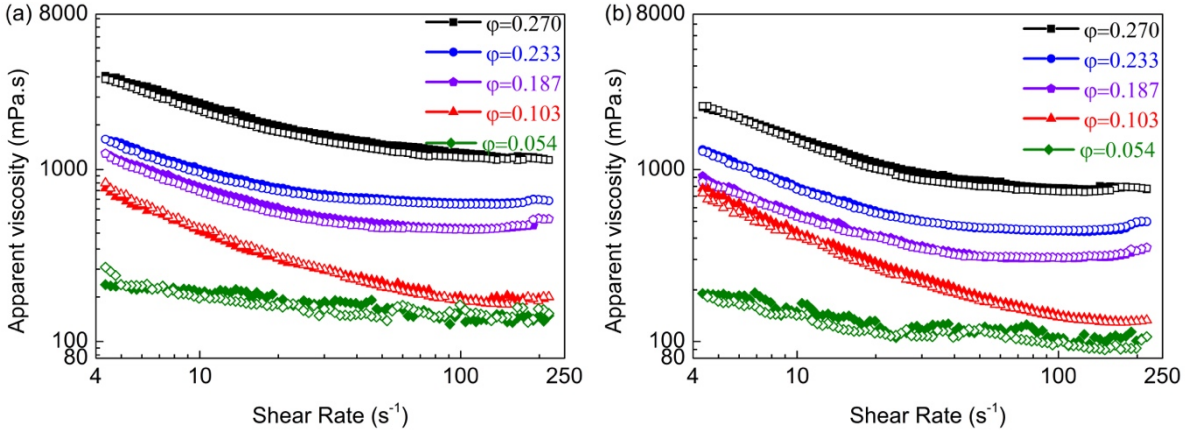

Figure 7. Steady state flow curves of hydrate slurries formed from water-in-oil B emulsions with AA and various different water cuts at 1 °C (Panel a) and 5 °C (Panel b). The initial methane pressure prior to hydrate formation and cooling was 10 MPa. Filled data points indicate increasing shear rate, while open data points correspond to decreasing shear rate.

Table 2. Cross fit parameters (eq (1)) for hydrate slurry flow curves formed from water-in-oil A emulsions with different water cuts, corresponding to the data presented in **Figure 6**.

Temperature	Hydrate Volume Fraction	η_∞ $(mPa.s)$	η_0 $(mPa.s)$	K (s)	m
1 °C	0.261	181.1	7736	0.925	1.45
	0.187	76.25	3103	0.808	1.36
	0.140	28.16	1301	0.305	1.33
	0.084	24.59	2578	0.697	1.28
	0.047	20.34	9631	3.043	1.29
5 °C	0.261	117.2	13951	4.499	1.20
	0.187	72.93	466439	32.60	1.42
	0.140	34.03	1107	0.342	1.41
	0.084	11.58	783	0.275	1.46
	0.047	7.851	4278	1.524	1.31

Table 3. Cross fit parameters (eq (1)) for hydrate slurry flow curves formed from water-in-oil B emulsions with different water cuts, corresponding to the data presented in **Figure 7**.

Temperature	Hydrate Volume Fraction	η_∞ $(mPa.s)$	η_0 $(mPa.s)$	K (s)	m
1 °C	0.270	1082	8864	0.509	1.10
	0.233	627.3	3011	0.338	1.52
	0.187	454.5	1895	0.223	1.75
	0.103	139.7	54760	29.82	0.90
	0.054	127.5	213.3	0.039	1.29
5 °C	0.270	743.8	3336	0.173	1.76
	0.233	447.4	1872	0.196	1.81
	0.187	309.1	1186	0.179	1.78

	0.103	103.4	3911	1.421	0.93
	0.054	93.20	409385	3511	0.87

Compared to the system without AA, the apparent viscosity of the hydrate slurries with AA was much lower at each shear rate tested, with one example shown in **Figure 8** illustrating an order-of-magnitude decrease in relative viscosity at 0.20 water cut; this was consistent with observations made during the hydrate formation process (**Figure 3**). At high shear rates, the flow curve for the system with AA tended to reach an apparent Newtonian region (e.g. above approximately 100 s^{-1} in **Figure 8**). These flow curves suggest that, under high shear conditions and with the addition of AA, hydrate particles may no longer aggregate in flow; under these conditions, the infinite shear rate viscosities were used as a basis with which to assess the accuracy of the underlying model for hydrate suspension proposed by Camargo and Palermo.[23]

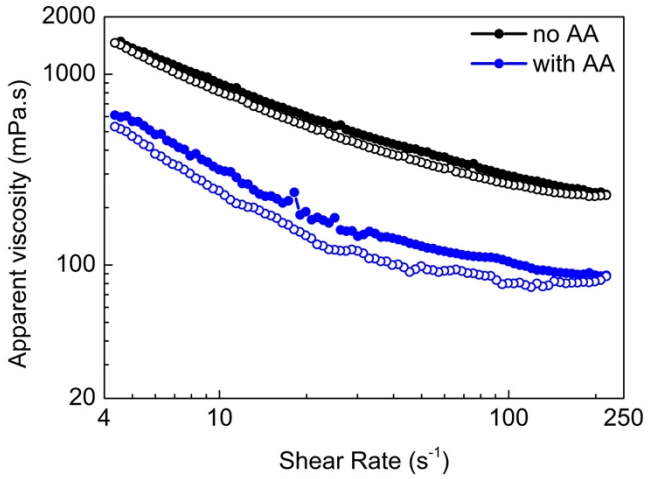

Figure 8. Steady state flow curves of hydrate slurries at 1 °C formed from water-in-oil A emulsions of 0.20 water cut, with and without AA. The initial methane pressure prior to hydrate formation and cooling was formed from an initial methane pressure of 10 MPa. Open data points correspond to decreasing shear rate.

3.3 Infinite Shear Viscosity of Hydrate Slurries with AA

By fitting the flow curve data of hydrate slurries with AA with the Cross model – Equation 1 [13], (an example shown in **Figure 9** Panel a), the infinite shear viscosities of hydrate suspensions with different hydrate volume fractions were collected for both oil A and oil B systems. As the state of hydrate particles in suspensions with infinite shear viscosity could be regarded as separated without aggregating, these relative viscosity data could be compared with the original underlying Mills model,[30] as well as some other widely used concentrated suspension models[43-46] (**Figure 9** panel b).

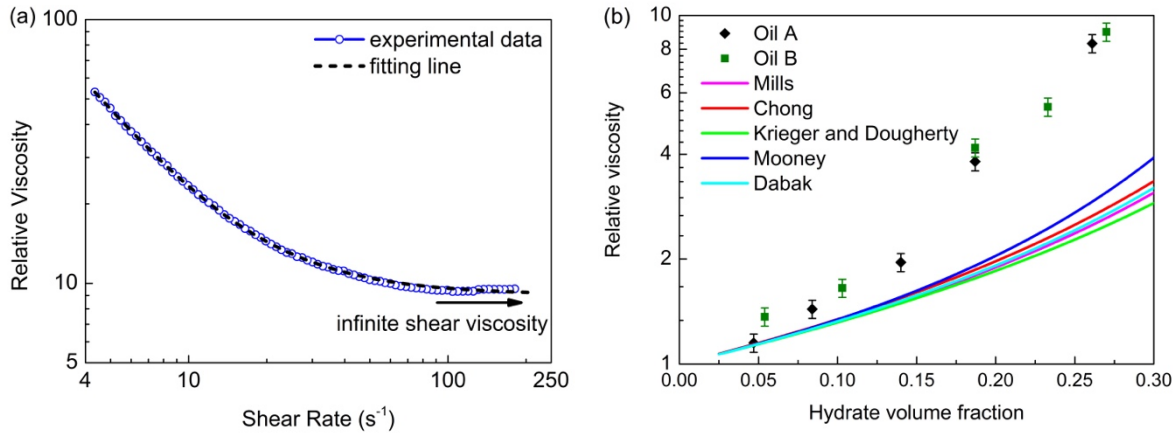

Figure 9. Infinite relative shear viscosity of hydrate slurries formed from water-in-oil A and B, with AA. Determination of infinite shear viscosity at 1 °C (Panel a), and comparison of values obtained for various hydrate volume fractions at 1 °C with the predictions of five different suspension models (Panel b).[45]

While the two data sets from different crude oils showed consistent behaviour (**Figure 9**), the deviation between these experimental data and the values predicted by the five models was substantial, especially for hydrate volume fractions above 0.15. This observation suggests that these suspension models may not be suitable to describe hydrate systems, which may the consequence of the models' consistent assumption of mono-sized, rigid spheres. In reality, hydrate particles formed in liquid hydrocarbon are neither rigid nor spherical – their shape can, in fact, become ellipsoidal due to the shear stress under flow. During the conversion process, dendrites can form on the surface of the hydrate particle, further increasing roughness; an example of hydrate particle roughness is shown in panels A and B of **Figure 10**, captured using a micromechanical force apparatus[48-49] for particles with and without AA, respectively. The deformation and roughness of the particles can result in additional energy dissipation during flow and a corresponding increase in apparent viscosity[50] compared to the rigid sphere system. Such deformational effects should be considered when attempting to describe the rheological properties of hydrate particle suspensions.

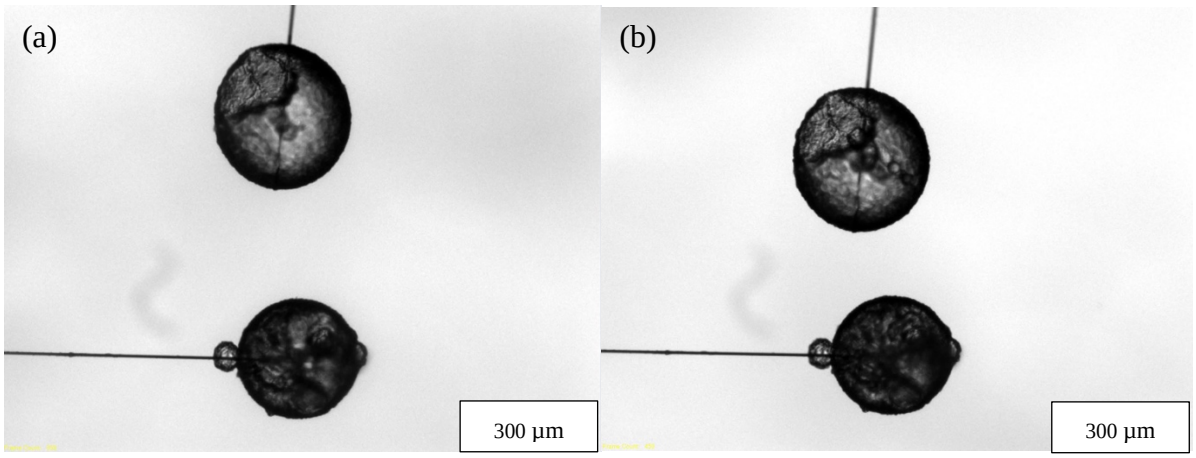

Figure 10. Photographs of cyclopentane hydrate particles in the liquid hydrocarbon phase without AA (Panel A) and with AA (Panel b).

One model for concentrated suspensions of arbitrarily-shaped particles was established by Santamaría-Holek and Mendoza[51] based on extended differential effective medium theories (DEMT):

$$\eta_r = [1 - \frac{\Phi}{1 - c * \Phi}]^{-[\eta]} \quad (2)$$

where η_r is the suspension's relative viscosity (suspension viscosity divided by the continuous phase viscosity); Φ is the volume fraction of the particles; $[\eta]$ is the intrinsic viscosity, determined by the particle shape; and c represents a crowding factor, defined as:

$$c = \frac{1 - \Phi_c}{\Phi_c} \quad (3)$$

where Φ_c is the filling fraction at which the suspension loses its fluidity, which is less than or equal to the maximum packing fraction Φ_{max} used by Mills.[30] By fitting the infinite shear viscosity data obtained for both oil systems, $[\eta]$ was estimated with a best fit of 5, while Φ_c was estimated with a best fit of 0.52. **Figure 11** shows a comparison of the data to the relative viscosities calculated with the model using these parameter values in the DEMT model.

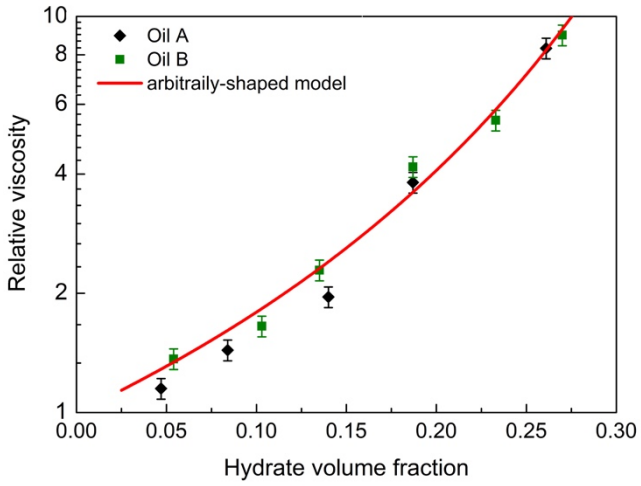

Figure 11. Infinite relative shear viscosity of hydrate slurries formed in oils A and B with the AA for different hydrate volume fractions at 1 °C, together with values calculated using the arbitrarily-shaped particle suspension model,[51] eq (2) and (3), with $[\eta]$=5 and Φ_c=0.52.

3.4 Development of a New Hydrate Slurry Rheology Model

With the improved accuracy of the extended DEMT model to describe non-aggregating suspension behavior, the mathematical treatment introduced by Camargo and Palermo[23] may be overlaid with two assumptions: (i) hydrate aggregates are fractal in nature; and (ii) the maximum aggregate size achieved in flow is controlled by a force balance of flowing shear

stress and inter-particle cohesive force. The maximum stable aggregate size (d_A) using this treatment can be estimated through equation (4):

$$\left(\frac{d_A}{d_p}\right)^{(4-f)} - \frac{F_a\left[1 - \frac{\Phi\left(\frac{d_A}{d_p}\right)^{(3-f)}}{1 - \Phi\left(\frac{1-\Phi_c}{\Phi_c}\right)\left(\frac{d_A}{d_p}\right)^{(3-f)}}\right]^{[\eta]}}{{d_p}^2 \eta_{oil} \dot{\gamma}} = 0 \quad (4)$$

where d_A is the hydrate aggregate diameter; d_p is the hydrate particle diameter; f is the fractal dimension; F_a is the force of cohesion between particles (measured to be a constant 4.3 mN/m when reduced by the mean hydrate particle diameter [2]); η_{oil} is the viscosity of methane saturated oil; and $\dot{\gamma}$ is the shear rate applied.

Upon solution of eq (4) for the aggregate size, the effective volume fraction (Φ_{eff}) can be calculated using equation (5).[23] This is required to determine the relative viscosity of the slurry containing hydrate aggregates using equation (6), which is derived from equations (2) and (3) by considering the effective volume fraction occupied by the aggregates.

$$\Phi_{eff} = \Phi\left(\frac{d_A}{d_p}\right)^{(3-f)} \quad (5)$$

$$\eta_r = \left[1 - \frac{\Phi_{eff}}{1 - \left(\frac{1-\Phi_c}{\Phi_c}\right) * \Phi_{eff}}\right]^{-[\eta]} \quad (6)$$

The DEMT model with Camargo and Palermo's mathematical treatment[23] was next compared with flow curves for hydrate suspensions in oils A and B in the absence of AA (panels A and B of **Figure 12**, respectively). For each calculation, the particle diameter d_p used in the calculation was based on low-field NMR measurements of mean water droplet size, and the hydrate volume fraction was determined by the measured pressure decrease during the experiment; these data are provided in **Table 4** for oil A and **Table 5** for oil B, with the methane saturated oil viscosities given in **Table 1**.

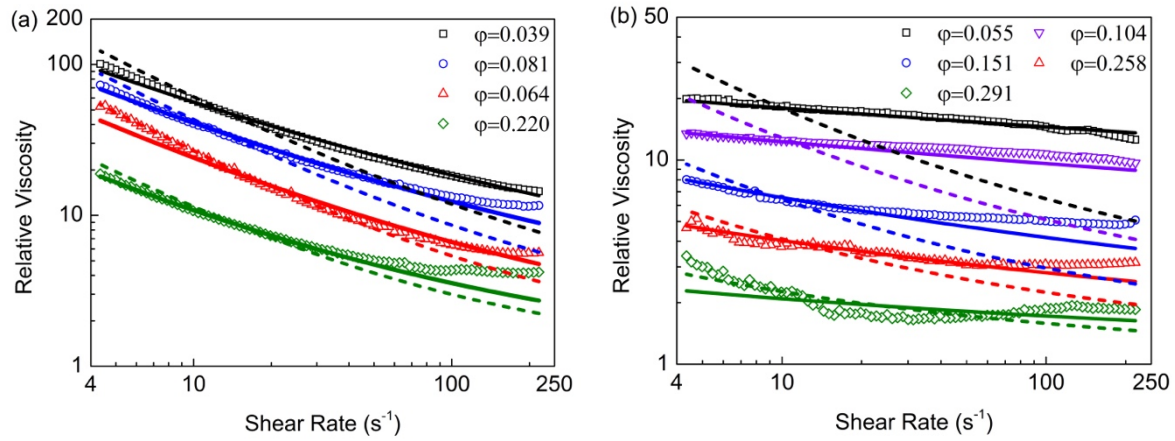

Figure 12. Comparison between experimental (open data points) hydrate slurry flow curves without AA and model predictions (lines) at different hydrate volume fractions at 1 °C for oil A (Panel a) and oil B (Panel b), where the solid lines correspond to predictions from the new model with the best-fit fractal dimension, and the dashed lines correspond to predictions from the original model by Camargo and Palermo[23] with the best-fit fractal dimension.

The intrinsic viscosity $[\eta]$ and filling fraction Φ_c were maintained at 5 and 0.52 respectively (**Figure 11**). The best-fit fractal dimensions ranged from 2.47 to 2.97, similar to the singular best-fit value of 2.5 proposed by Camargo and Palermo.[23] Average absolute deviations for both models are reported in **Table 6** for oil A and **Table 7** for oil B, which indicates that the accuracy of the model developed in this work is superior to that of the original model. With these improvements to the underlying suspension viscosity model, future work may consider revisions to the particle aggregation methods that are deployed in both this approach and that of Camargo and Palermo.

Table 4. Particle diameter and final hydrate volume fractions for non-AA tests with oil A.

Water cut	0.05	0.10	0.20	0.30
Hydrate volume fraction Φ	0.039	0.081	0.164	0.220
Particle diameter d_p (μm)	3.34	3.62	3.72	3.82

Table 5. Particle diameter and final hydrate volume fractions for non-AA tests with oil B.

Water cut	0.05	0.10	0.15	0.25	0.30
Hydrate volume fraction Φ	0.055	0.104	0.151	0.258	0.291
Particle diameter d_p (μm)	1.70	2.03	2.75	3.30	3.30

Table 6. Best-fit fractal dimension and average absolute deviation for both suspension models applied to hydrate suspensions with oil A at 1°C at four hydrate volume fractions.

Hydrate volume fraction Φ	Camargo and Palermo Model [23]		Extended DEMT-Based Model	
	f (best fit)	Average Deviation Between Model and Experiment (%)	f (best fit)	Average Deviation Between Model and Experiment (%)
0.039	2.24	17.48	2.47	8.42
0.081	2.38	8.29	2.59	7.8
0.164	2.63	20.64	2.78	4.8
0.220	2.71	20.63	2.85	3.17

Table 7. Best-fit fractal dimension and average absolute deviation for both suspension models applied to hydrate suspensions with oil B at 1°C at four hydrate volume fractions.

Hydrate volume fraction Φ	Original Camargo and Palermo model		Extended DEMT-Based Model	
	f (best fit)	Average Deviation Between Model and Experiment (%)	f (best fit)	Average Deviation Between Model and Experiment (%)
0.055	2.70	10.2	2.86	10.73
0.104	2.73	16.84	2.87	5.14
0.151	2.75	24.54	2.89	8.55
0.258	2.83	34.7	2.97	6.08
0.291	2.84	36.65	2.98	2.28

3.5 Yield Stress of Hydrate-in-Oil Slurries

Following flow curve tests, systems with and without AA were exposed to an eight-hour annealing period to simulate the shut-in process of an industrial pipeline. Following this period, the yield stress of hydrate slurries was measured with the procedure described above,[11-12, 14] using the same analysis procedure described previously by Qin et al.[40] The yield stress of hydrate-in-oil A slurries with AA was measured at 5 °C for water cuts ranging from

0.05 to 0.3. The results are compared in **Figure 13** with measurements of the system without AA, against a benchmark of ketchup at 20 °C.[52] For both hydrate systems, the yield stress increased with increasing water cut; however, the addition of AA maintained all yield stress values below 5 Pa, constituting an 80% decrease from the non-AA system at a water cut of 0.30. This result suggests that the addition of AA may also provide a positive benefit to operators when restarting hydrated oil systems.

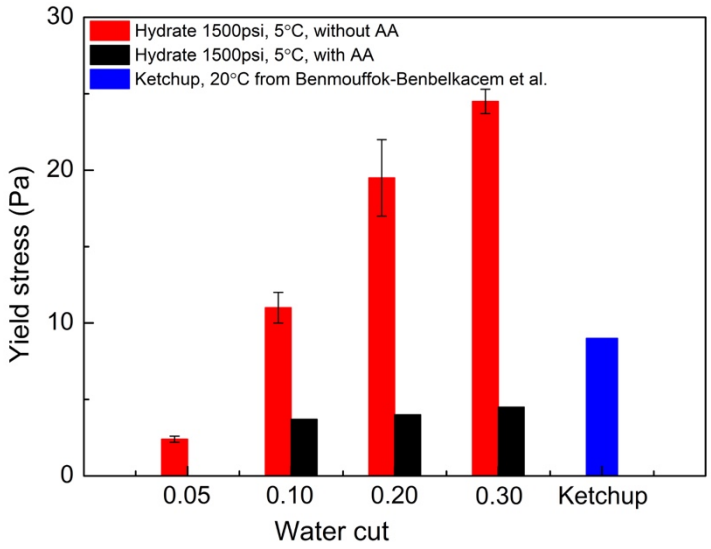

Figure 13. Yield stress of hydrate slurries formed from water-in-oil A emulsions without AA (red) and with AA (black) of 0.05, 0.10, 0.20 and 0.30 water cut, following an eight-hour annealing period at 5 °C; the yield stress of ketchup at 20 °C (blue)[52] is shown for comparative purposes.

4 CONCLUSIONS

The rheological properties of hydrate slurries formed from water-in-oil emulsions with AA were tested using a controlled-stress rheometer in two crude oil systems. During hydrate formation and at constant shear rate, the pressure, temperature and apparent viscosity profiles of the systems were recorded under isochoric conditions. The volume fraction of methane hydrate in oil was quantified through the measured pressure decrease. At the same water cut, the addition of AA resulted in order-of-magnitude decreases in both hydrate growth rate and apparent viscosity, while the AA did not affect the extent of water conversion at steady-state. Further, the addition of AA reduced the yield stress of hydrate slurries by approximately 80% for water cuts between 0.1 and 0.3.

The flow curves for steady-state hydrate-in-oil slurries were measured at 1 and 5 °C after cessation of the hydrate reaction. The addition of AA resulted in apparent viscosities that were minimally dependent on shear rate above 100 s^{-1}, suggesting the presence of a non-

aggregating suspension; the apparent viscosity observed in these regions deviated by up to factor of five from the currently-used suspension model by Mills.[28]

A revised DEMT-based formulation of the hydrate slurry viscosity model was derived, considering rough, arbitrarily-shaped particles. Allowing the fractal dimension to be used as a fitting parameter for both the current and the extended DEMT-based models, the latter improved AAD for two crude oil systems by between 50 and 60%.

Acknowledgements

The authors acknowledge the Australian Research Council and Woodside Energy Ltd. for support of this work through Linkage project LP150100785. The purchase of the rheometer was supported in part by the National Geosequestration Laboratory (NGL). Z.M. Aman acknowledges Chevron and Woodside for their support of the Professorial Chair in Long Subsea Tiebacks.

Reference

1. Sloan Jr, E. D.; Koh, C., *Clathrate hydrates of natural gases*. CRC press: 2007.
2. Aman, Z. M.; Brown, E. P.; Sloan, E. D.; Sum, A. K.; Koh, C. A., Interfacial mechanisms governing cyclopentane clathrate hydrate adhesion/cohesion. *Physical Chemistry Chemical Physics* **2011,** *13* (44), 19796-19806.
3. Webb, E. B.; Rensing, P. J.; Koh, C. A.; Sloan, E. D.; Sum, A. K.; Liberatore, M. W., High pressure rheometer for in situ formation and characterization of methane hydrates. *Review of Scientific Instruments* **2012,** *83* (1).
4. Sloan, E. D.; Koh, C. A.; Sum, A., *Natural gas hydrates in flow assurance*. Gulf Professional Publishing: 2010.
5. Turner, D. J. Clathrate hydrate formation in water-in-oil dispersions. Colorado School of Mines Golden, CO, 2005.
6. Zerpa, L. E.; Sloan, E. D.; Koh, C.; Sum, A., Hydrate risk assessment and restart-procedure optimization of an offshore well using a transient hydrate prediction model. *Oil and Gas Facilities* **2012,** *1* (05), 49-56.
7. Norris, B. W. E.; Zerpa, L. E.; Koh, C. A.; Johns, M. L.; May, E. F.; Aman, Z. M., Rapid assessments of hydrate blockage risk in oil-continuous flowlines. *Journal of Natural Gas Science and Engineering* **2016,** *30*, 284-294.
8. Zylyftari, G.; Lee, J. W.; Morris, J. F., Salt effects on thermodynamic and rheological properties of hydrate forming emulsions. *Chemical Engineering Science* **2013,** *95*, 148-160.
9. Zylyftari, G.; Ahuja, A.; Morris, J. F., Modeling Oilfield Emulsions: Comparison of Cyclopentane Hydrate and Ice. *Energy & Fuels* **2015,** *29* (10), 6286-6295.
10. Ma, Z. W.; Zhang, P.; Wang, R. Z.; Furui, S.; Xi, G. N., Forced flow and convective melting heat transfer of clathrate hydrate slurry in tubes. *International Journal of Heat and Mass Transfer* **2010,** *53* (19–20), 3745-3757.
11. Webb, E. B.; Rensing, P. J.; Koh, C. A.; Sloan, E. D.; Sum, A. K.; Liberatore, M. W., High-Pressure Rheology of Hydrate Slurries Formed from Water-in-Oil Emulsions. *Energy & Fuels* **2012,** *26* (6), 3504-3509.

12. Webb, E. B.; Koh, C. A.; Liberatore, M. W., High Pressure Rheology of Hydrate Slurries Formed from Water-in-Mineral Oil Emulsions. *Industrial & Engineering Chemistry Research* **2014,** *53* (17), 6998-7007.
13. Cross, M. M., RHEOLOGY OF NON-NEWTONIAN FLUIDS - A NEW FLOW EQUATION FOR PSEUDOPLASTIC SYSTEMS. *Journal of Colloid Science* **1965,** *20* (5), 417-&.
14. Webb, E. B.; Koh, C. A.; Liberatore, M. W., Rheological Properties of Methane Hydrate Slurries Formed From AOT plus Water plus Oil Microemulsions. *Langmuir* **2013,** *29* (35), 10997-11004.
15. Herschel, W. H.; Bulkley, R. In *Measurement of consistency as applied to rubber-benzene solutions*, Am. Soc. Test Proc, 1926; pp 621-633.
16. Delahaye, A.; Fournaison, L.; Marinhas, S.; Martinez, M. C., Rheological study of CO2 hydrate slurry in a dynamic loop applied to secondary refrigeration. *Chemical Engineering Science* **2008,** *63* (13), 3551-3559.
17. Delahaye, A.; Fournaison, L.; Jerbi, S.; Mayoufi, N., Rheological properties of CO2 hydrate slurry flow in the presence of additives. *Industrial & Engineering Chemistry Research* **2011,** *50* (13), 8344-8353.
18. Bingham, E. C., *Fluidity and plasticity*. McGraw-Hill Book Compny, Incorporated: 1922; Vol. 2.
19. Darbouret, M.; Cournil, M.; Herri, J.-M., Rheological study of TBAB hydrate slurries as secondary two-phase refrigerants. *International Journal of Refrigeration* **2005,** *28* (5), 663-671.
20. Andersson, V.; Gudmundsson, J. S., Flow properties of hydrate ‐ in ‐ water slurries. *Annals of the New York Academy of Sciences* **2000,** *912* (1), 322-329.
21. Clain, P.; Delahaye, A.; Fournaison, L.; Mayoufi, N.; Dalmazzone, D.; Fuerst, W., Rheological Properties of tetra-n-butylphosphonium bromide hydrate slurry flow. *Chemical Engineering Journal* **2012,** *193*, 112-122.
22. Yan, K.-L.; Sun, C.-Y.; Chen, J.; Chen, L.-T.; Shen, D.-J.; Liu, B.; Jia, M.-L.; Niu, M.; Lv, Y.-N.; Li, N., Flow characteristics and rheological properties of natural gas hydrate slurry in the presence of anti-agglomerant in a flow loop apparatus. *Chemical Engineering Science* **2014,** *106*, 99-108.
23. Camargo, R.; Palermo, T., Rheological Properties of Hydrate Suspensions in an Asphaltenic Crude Oil. In *4th International Conference on Gas Hydrates*, 2002.
24. Sinquin, A.; Palermo, T.; Peysson, Y., Rheological and flow properties of gas hydrate suspensions. *Oil & gas science and technology* **2004,** *59* (1), 41-57.
25. Palermo, T.; Fidel-Dufour, A.; Maurel, P.; Peytavy, J.; Hurtevent, C. In *Model of hydrates agglomeration–Application to hydrates formation in an acidic crude oil*, 12th International Conference on Multiphase Production Technology, BHR Group: 2005.
26. Fidel-Dufour, A.; Gruy, F.; Herri, J.-M., Rheology of methane hydrate slurries during their crystallization in a water in dodecane emulsion under flowing. *Chemical Engineering Science* **2006,** *61* (2), 505-515.
27. Colombel, E.; Gateau, P.; Barré, L.; Gruy, F.; Palermo, T., Discussion of agglomeration mechanisms between hydrate particles in water in oil emulsions. *Oil & Gas Science and Technology-Revue de l'IFP* **2009,** *64* (5), 629-636.
28. Boxall, J., et al., *Predicting When and Where Hydrate Plugs Form in Oil-Dominated Flowlines.* SPE Projects, Facilities & Construction, 2009: p. 1-7.
29. Davies, S. R., Boxall, J. A., Dieker, L. E., Sum, A. K., Koh, C. A., Sloan, E. D., … Xu, Z. G. (2010). Predicting hydrate plug formation in oil-dominated flowlines. *Journal of Petroleum Science and Engineering*, *72*(3–4), 302–309. https://doi.org/10.1016/j.petrol.2010.03.031

30. Mills, P., Non-Newtonian behaviour of flocculated suspensions. *Journal de Physique Lettres* **1985,** *46* (7), 301-309.
31. Potanin, A. A., On the mechanism of aggregation in the shear flow of suspensions. *Journal of Colloid and Interface Science* **1991,** *145* (1), 140-157.
32. Hoekstra, L. L.; Vreeker, R.; Agterof, W. G. M., Aggregation of colloidal nickel hydroxycarbonate studied by light scattering. *Journal of Colloid and Interface Science* **1992,** *151* (1), 17-25.
33. Muehle, K., Floc stability in laminar and turbulent flow. *Surfactant Science Series* **1993**, 355-355.
34. Gmachowski, L., Estimation of the dynamic size of fractal aggregates. *Colloids and Surfaces A: Physicochemical and Engineering Aspects* **2000,** *170* (2–3), 209-216.
35. Kelland, M. A., History of the development of low dosage hydrate inhibitors. *Energy & Fuels* **2006,** *20* (3), 825-847.
36. Aman, Z. M.; Haber, A.; Ling, N. N.; Thornton, A.; Johns, M. L.; May, E. F., Effect of Brine Salinity on the Stability of Hydrate-in-Oil Dispersions and Water-in-Oil Emulsions. *Energy & Fuels* **2015,** *29* (12), 7948-7955.
37. Ling, N. N. A.; Haber, A.; May, E. F.; Fridjonsson, E. O.; Johns, M. L., NMR studies of emulsion microstructure approaching the phase inversion point. *Colloids and Surfaces A: Physicochemical and Engineering Aspects* **2014,** *462*, 244-251.
38. Johns, M. L., NMR studies of emulsion. *Current Opinion in Colloid & Interface Science* **2009,** *14* (3), 178-183.
39. Fridjonsson, E. O.; Graham, B. F.; Akhfash, M.; May, E. F.; Johns, M. L., Optimized Droplet Sizing of Water-in-Crude Oil Emulsions Using Nuclear Magnetic Resonance. *Energy & Fuels* **2014,** *28* (3), 1756-1764.
40. Qin, Y.; Aman, Z. M.; Pickering, P. F.; Johns, M. L.; May, E. F., High pressure rheological measurements of gas hydrate-in-oil slurries. *Journal of Non-Newtonian Fluid Mechanics* **2017,** *248*, 40-49.
41. Ballard, A. L.; Sloan, E. D., The next generation of hydrate prediction. IV: A comparison of available hydrate prediction programs. *Fluid Phase Equilibria* **2004,** *216* (2), 257-270.
42. Aman, Z. M.; Koh, C. A., Interfacial phenomena in gas hydrate systems. *Chemical Society Reviews* **2016**.
43. Chong, J. S.; Christiansen, E. B.; Baer, A. D., Rheology of concentrated suspensions. *Journal of applied polymer science* **1971,** *15* (8), 2007-2021.
44. Krieger, I. M.; Dougherty, T. J., A mechanism for non‐Newtonian flow in suspensions of rigid spheres. *Transactions of the Society of Rheology* **1959,** *3* (1), 137-152.
45. Mooney, M., The viscosity of a concentrated suspension of spherical particles. *Journal of colloid science* **1951,** *6* (2), 162-170.
46. Dabak, T.; Yucel, O., Shear viscosity behavior of highly concentrated suspensions at low and high shear-rates. *Rheologica Acta* **1986,** *25* (5), 527-533.
47. Senapati, P. K.; Panda, D.; Parida, A., Predicting Viscosity of Limestone-Water Slurry. *Journal of Minerals & Materials Characterization & Engineering* **2009,** *8* (3), 203-221.
48. Morrissy, S. A.; Lim, V. W.; May, E. F.; Johns, M. L.; Aman, Z. M.; Graham, B. F., Micromechanical Cohesive Force Measurements Between Precipitated Asphaltene Solids and Cyclopentane Hydrates. *Energy & Fuels* **2015,** *29* (10), 6277-6285.

49. Morrissy, S. A.; McKenzie, A. J.; Graham, B. F.; Johns, M. L.; May, E. F.; Aman, Z. M., Reduction of Clathrate Hydrate Film Growth Rate by Naturally Occurring Surface Active Components. *Energy & Fuels* **2017,** *31* (6), 5798-5805.
50. Genovese, D. B., Shear rheology of hard-sphere, dispersed, and aggregated suspensions, and filler-matrix composites. *Advances in colloid and interface science* **2012,** *171*, 1-16.
51. Santamarı´a-Holek, I.; Mendoza, C. I., The rheology of concentrated suspensions of arbitrarily-shaped particles. *Journal of Colloid and Interface Science* **2010,** *346* (1), 118-126.
52. Benmouffok-Benbelkacem, G.; Caton, F.; Baravian, C.; Skali-Lami, S., Non-linear viscoelasticity and temporal behavior of typical yield stress fluids: Carbopol, Xanthan and Ketchup. *Rheologica acta* **2010,** *49* (3), 305-314.